

## Supporting information

### Structural optimization of ZIF-8-derived porous N-doped carbon materials for effective CO<sub>2</sub> capture

Hao Wang, Jiadi Gao, Xianyi Liu, Zhiguo Zhang, Zhigeng Fan, Yange Suo\*

School of Mechanical and Energy Engineering, Zhejiang University of Science and  
Technology, Liuhe Road 318#, Hangzhou, Zhejiang Province 310023, China  
E-mail address: suoyange@zust.edu.cn (Yange Suo);

Standardized formula for multiple linear regression equations:

$$\sigma = \sqrt{\frac{\sum(x_i - \mu)^2}{n}} \quad (S1)$$

$$z_i = \frac{x_i - \mu}{\sigma} \quad (S2)$$

where  $\sigma$  denotes the variance,  $\mu$  denotes the mean, and  $z$  denotes the data after standardization.

Dual-site Langmuir-Freundlich model equation is as follows [1]:

$$q = q_c \frac{K_c p}{1 + K_c p} + q_i \frac{K_i p}{1 + K_i p}$$

(S3)

Where, “ $q$ ” denotes the amount adsorbed in unit of mmol g<sup>-1</sup>, “ $q_c$ ” and “ $q_i$ ” represent saturation capacity of the two adsorption sites in unit of mmol g<sup>-1</sup>, respectively. “ $K_c$ ” and “ $K_i$ ” is DSLF fitting parameters of the two adsorption sites in unit of bar<sup>-1</sup>, respectively.

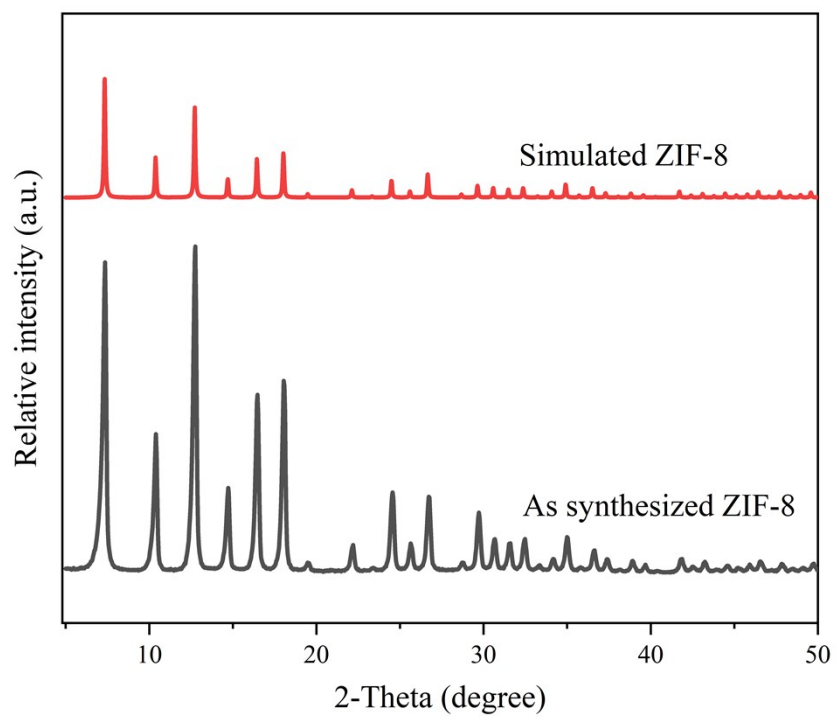


**Figure S1.** XRD patterns of the simulated ZIF-8 and the as-synthesized ZIF-8.

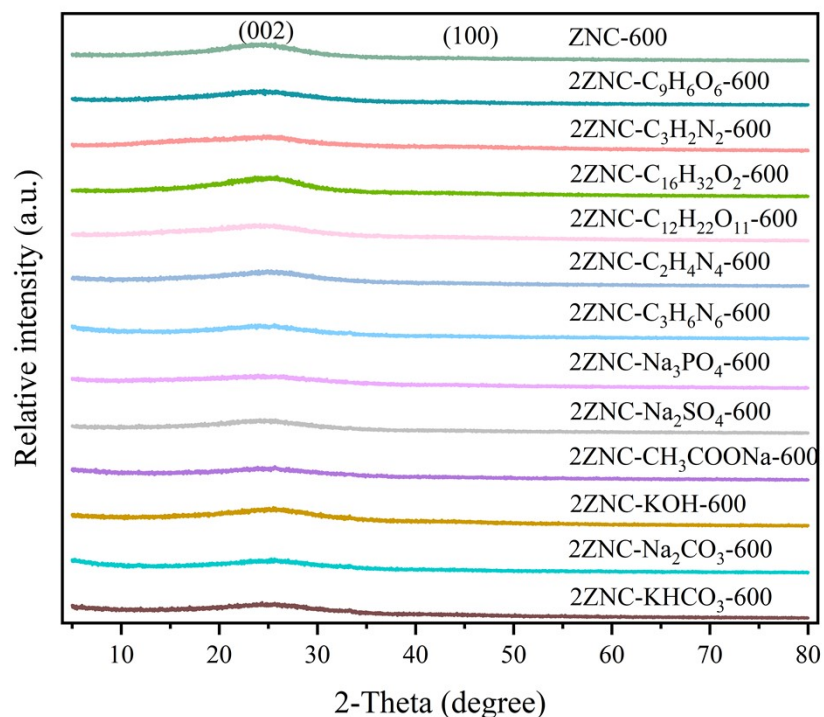


**Figure S2.** XRD patterns of ZNCs.

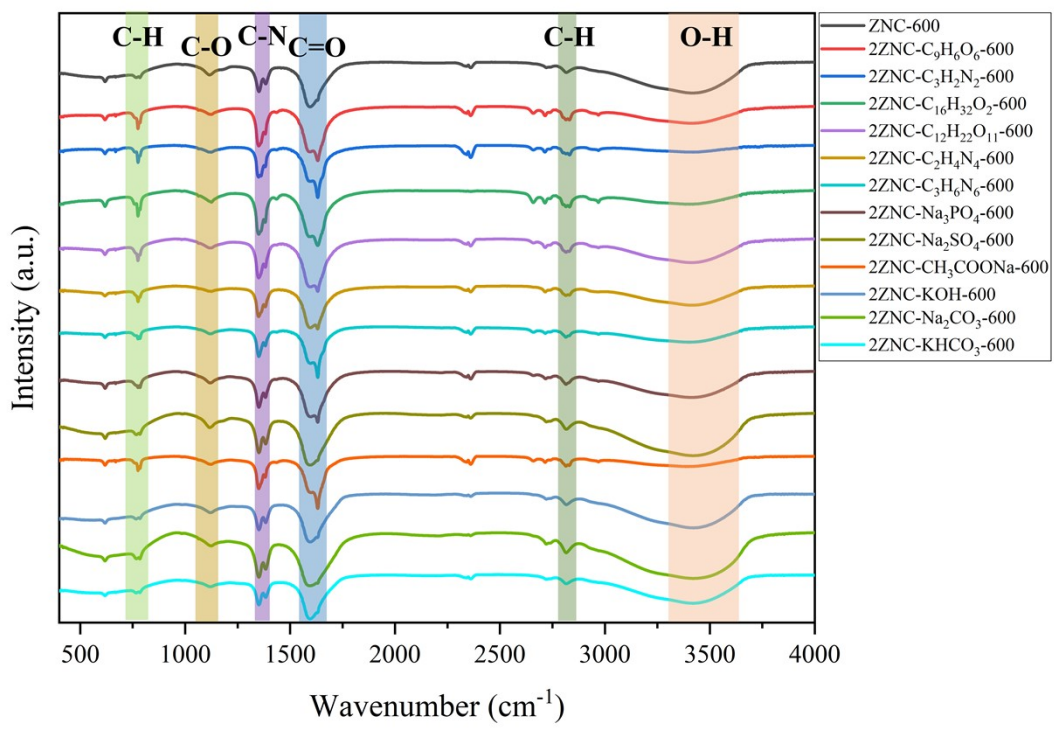


**Figure S3.** FTIR spectrum of ZNCs.

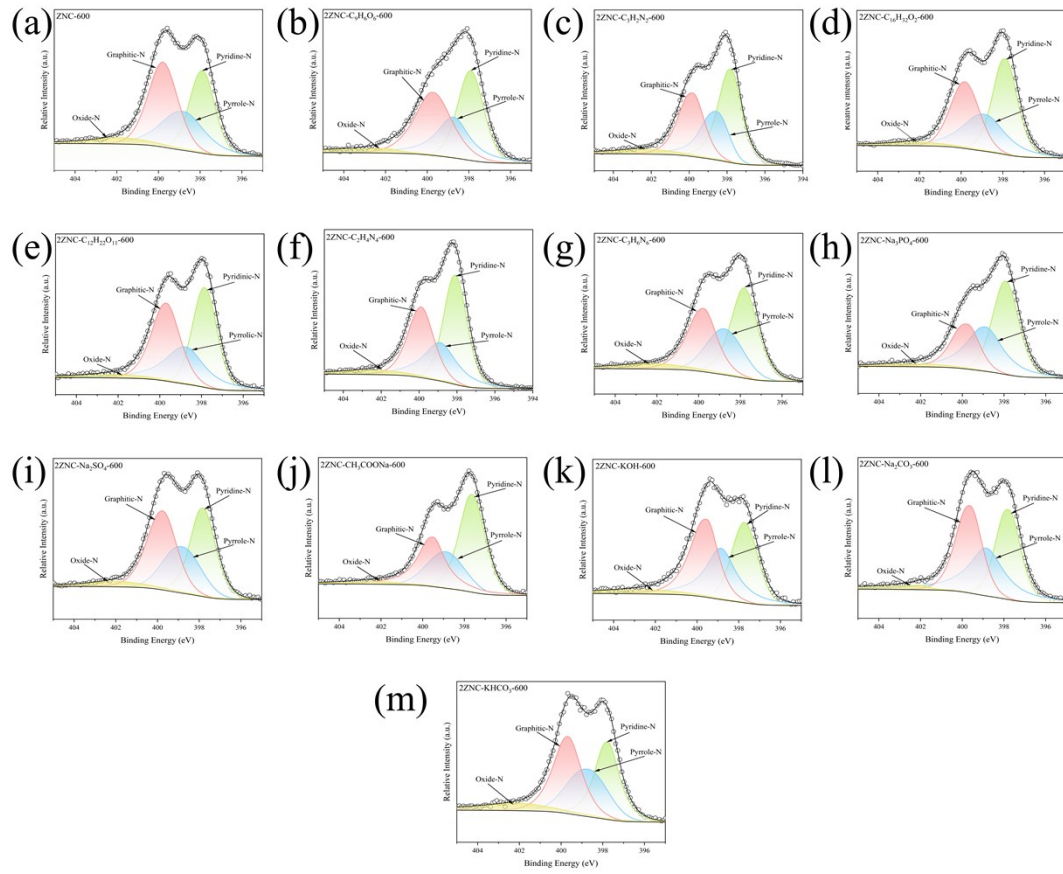


**Figure S4.** N1s spectrum of (a) ZNC-600, (b) 2ZNC-C<sub>9</sub>H<sub>6</sub>O<sub>6</sub>-600, (c) 2ZNC - C<sub>3</sub>H<sub>2</sub>N<sub>2</sub>-600, (d) 2ZNC-C<sub>16</sub>H<sub>32</sub>O<sub>2</sub>-600, (e) 2ZNC-C<sub>12</sub>H<sub>22</sub>O<sub>11</sub>-600, (f) 2ZNC-C<sub>2</sub>H<sub>4</sub>N<sub>4</sub>-600, (g) 2ZNC-C<sub>3</sub>H<sub>6</sub>N<sub>6</sub>-600, (h) 2ZNC-Na<sub>3</sub>PO<sub>4</sub>-600, (i) 2ZNC-Na<sub>2</sub>SO<sub>4</sub>-600, (j) 2ZNC-CH<sub>3</sub>COONa-600, (k) 2ZNC-KOH-600, (l) 2ZNC-Na<sub>2</sub>CO<sub>3</sub>-600, (m) 2ZNC-KHCO<sub>3</sub>-600.

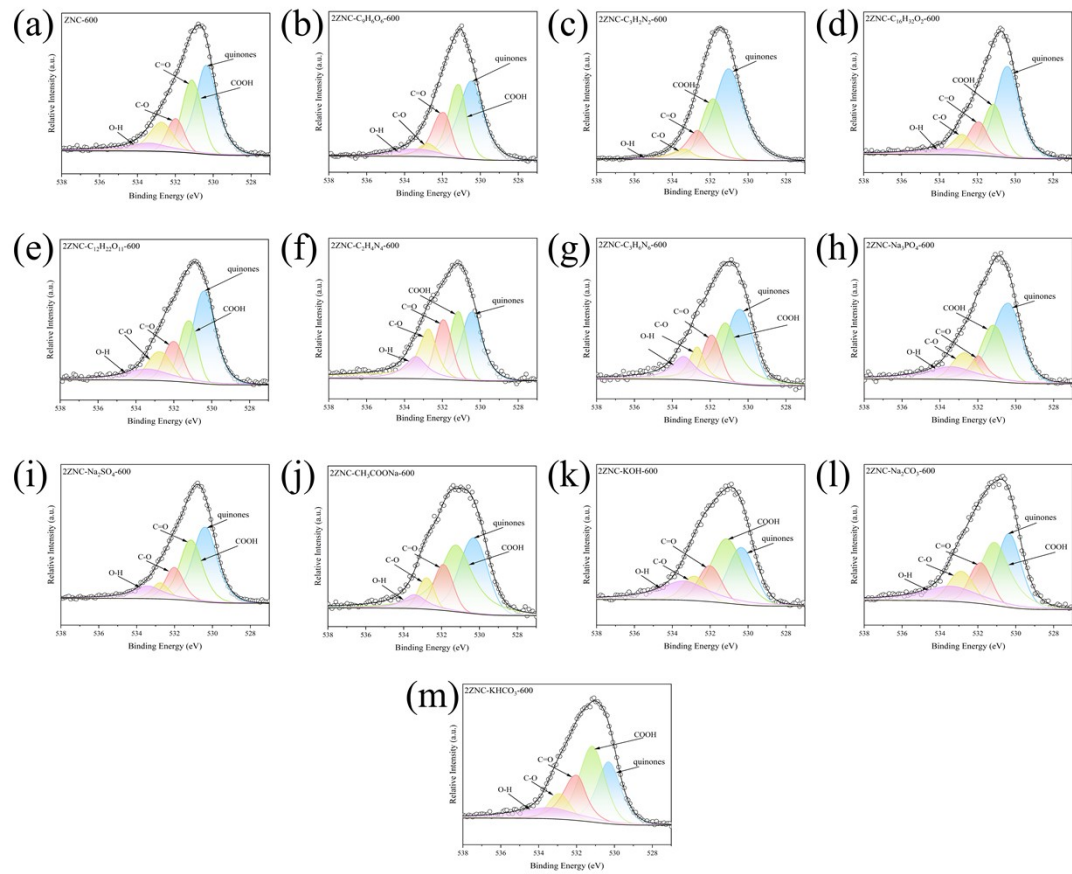


**Figure S5.** O1s spectrum of (a) ZNC-600, (b) 2ZNC-C<sub>9</sub>H<sub>6</sub>O<sub>6</sub>-600, (c) 2ZNC - C<sub>3</sub>H<sub>2</sub>N<sub>2</sub>-600, (d) 2ZNC-C<sub>16</sub>H<sub>32</sub>O<sub>2</sub>-600, (e) 2ZNC-C<sub>12</sub>H<sub>22</sub>O<sub>11</sub>-600, (f) 2ZNC-C<sub>2</sub>H<sub>4</sub>N<sub>4</sub>-600, (g) 2ZNC-C<sub>3</sub>H<sub>6</sub>N<sub>6</sub>-600, (h) 2ZNC-Na<sub>3</sub>PO<sub>4</sub>-600, (i) 2ZNC-Na<sub>2</sub>SO<sub>4</sub>-600, (j) 2ZNC-CH<sub>3</sub>COONa-600, (k) 2ZNC-KOH-600, (l) 2ZNC-Na<sub>2</sub>CO<sub>3</sub>-600, (m) 2ZNC-KHCO<sub>3</sub>-600.

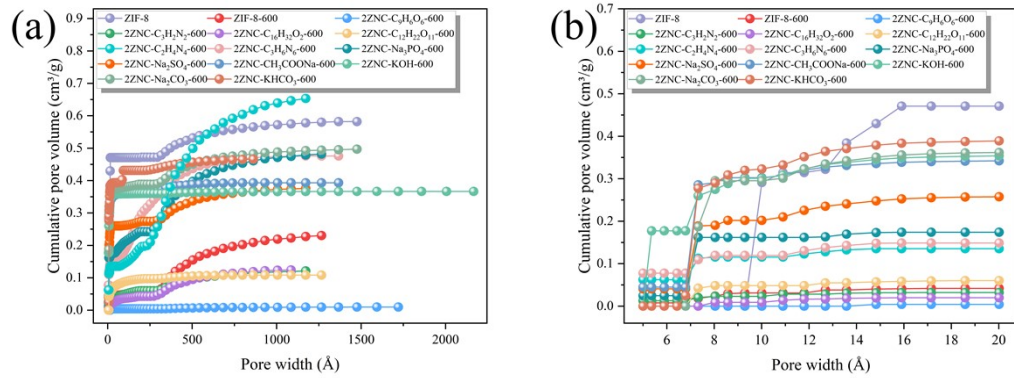


**Figure S6.** (a) Cumulative pore volume of ZIF-8 and ZNCs; (b) Cumulative pore volume of ZIF-8 and ZNCs in the pore size range of 0-20  $\text{\AA}$ .

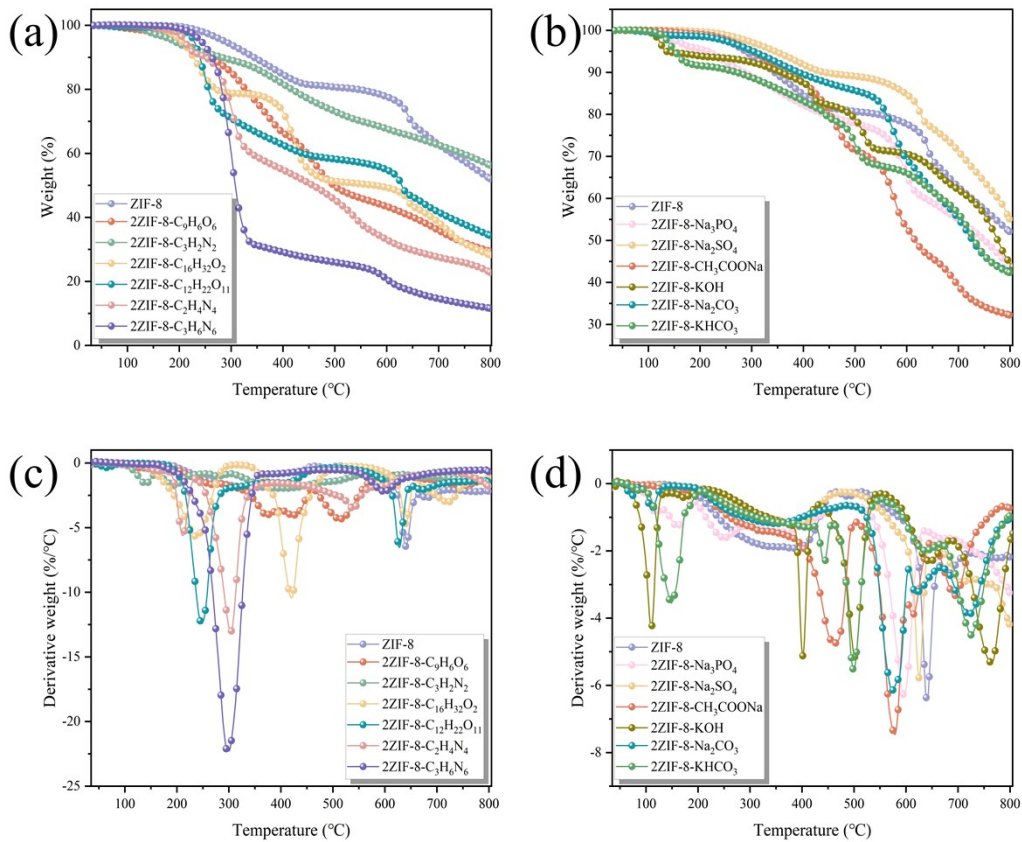


**Figure S7.** (a) TG curves of ZIF-8 and 2ZNC-organic compounds; (b) TG curves of ZIF-8 and 2ZNC-inorganic compounds; (c) DTG curves of ZIF-8 and 2ZNC-organic compounds; (b) DTG curves of ZIF-8 and 2ZNC-inorganic compounds.

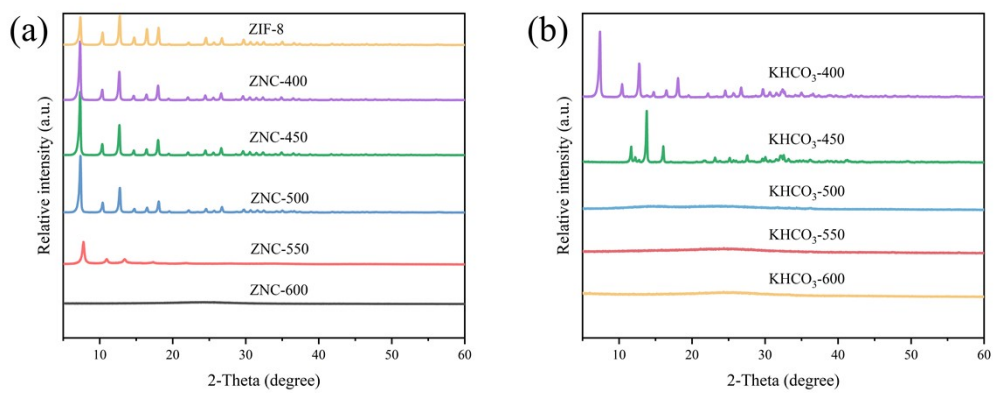


**Figure S8.** (a) XRD patterns of the ZIF-8 and ZNC-T (400-600°C); (b) XRD patterns of the 2ZNC-KHCO<sub>3</sub>-T (400-600°C).

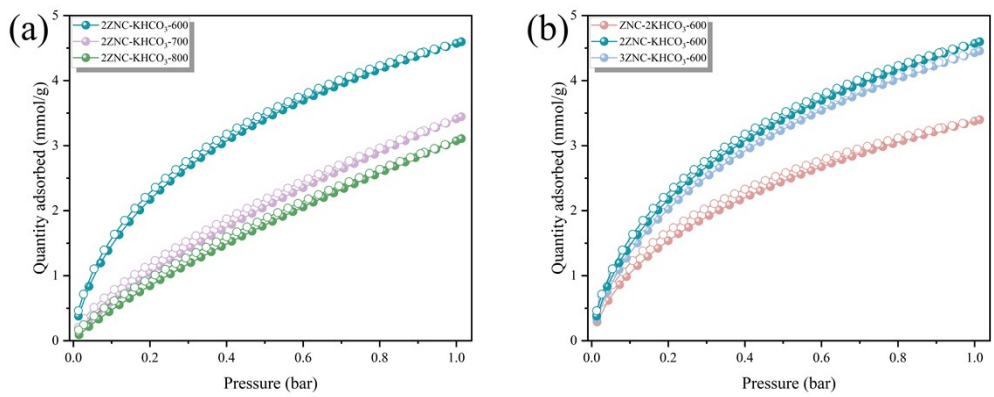


**Figure S9.** (a) The CO<sub>2</sub> adsorption capacity of 2ZNC-KHCO<sub>3</sub>-T at 25 °C and 1 bar;  
(b) The CO<sub>2</sub> adsorption capacity of xZNC-yKHCO<sub>3</sub>-600 at 25 °C and 1 bar.

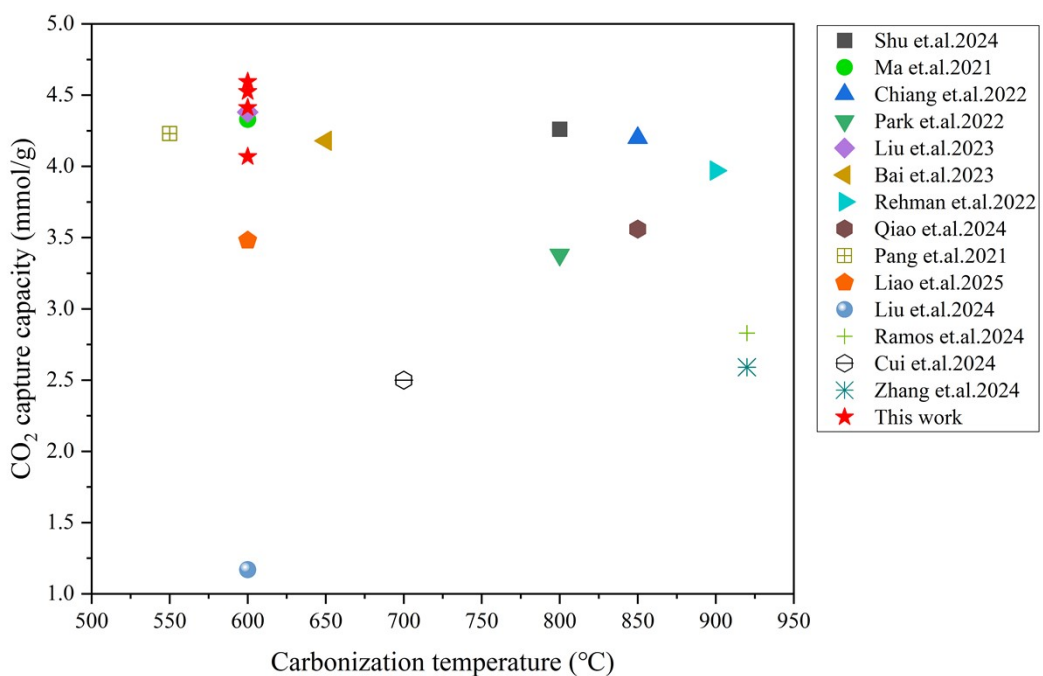


**Figure S10.** Comparison of  $\text{CO}_2$  adsorption capacity of ZNCs from this paper and other carbon materials from existing literature (at 1 bar and  $25^{\circ}\text{C}$ ).

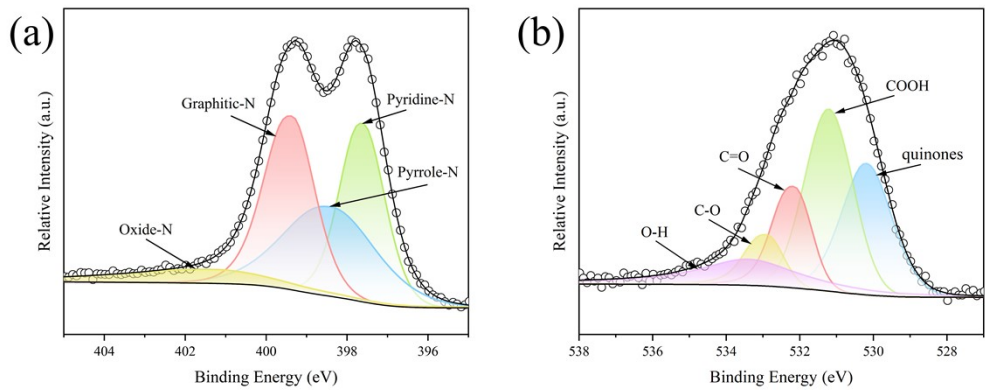


**Figure S11.** (a) N1s spectra of 2ZNC-KHCO<sub>3</sub>-600 after CO<sub>2</sub> adsorption; (b) O1s spectra of 2ZNC-KHCO<sub>3</sub>-600 after CO<sub>2</sub> adsorption.

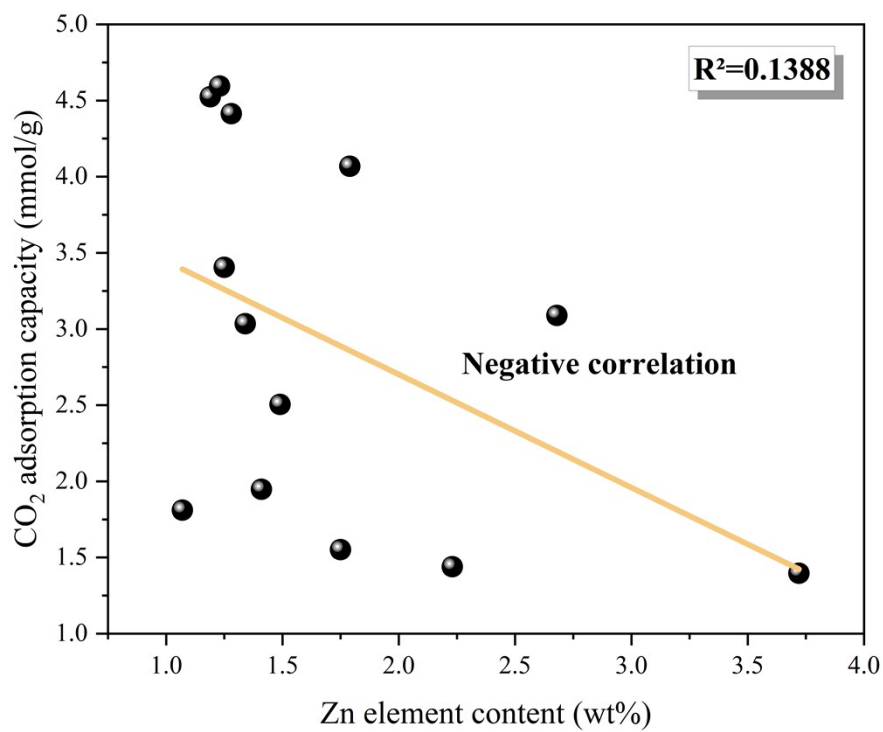


**Figure S12.** The linear correlation analyses between the CO<sub>2</sub> adsorption capacities (at 25 °C and 1 bar) and contents of Zn element.

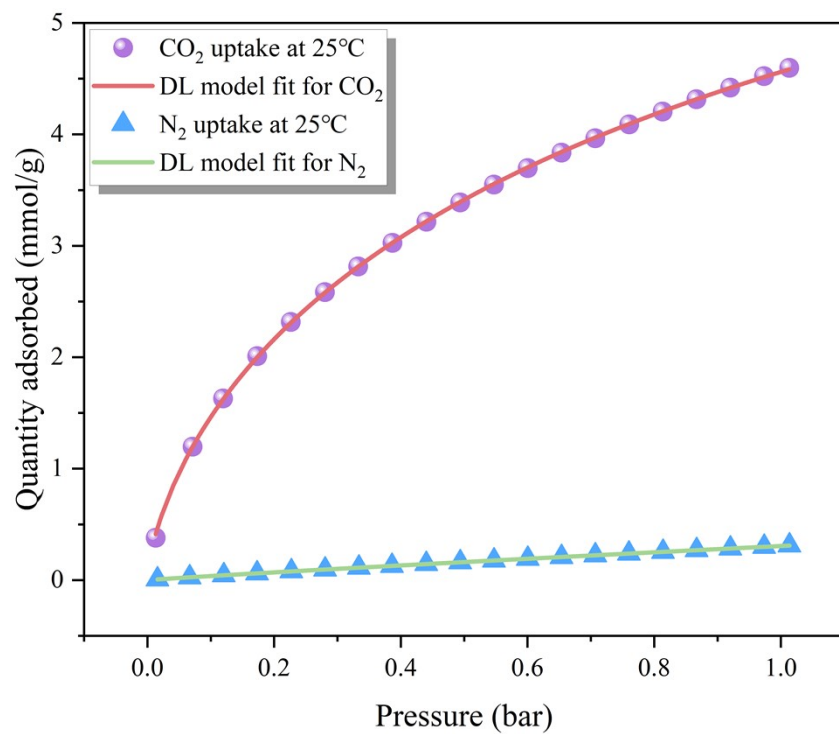


**Figure S13.** CO<sub>2</sub> and N<sub>2</sub> adsorption for 2ZNC-KHCO<sub>3</sub>-600 fitted by Dual-site Langmuir Freundlich model measured at 25°C.

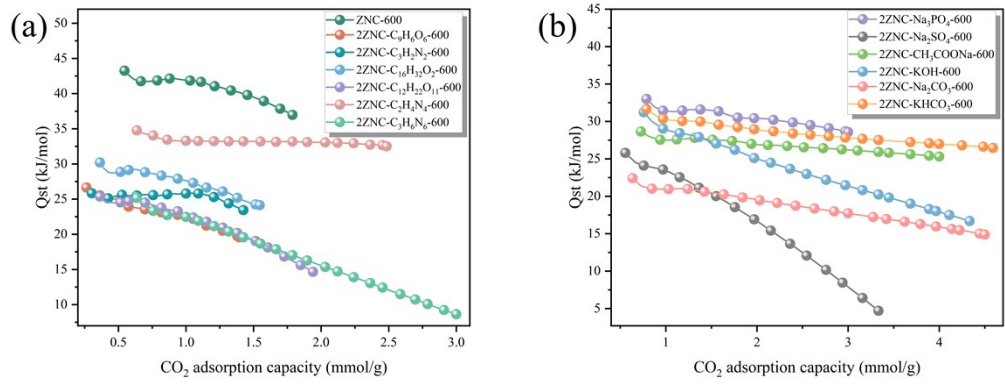


**Figure S14.** (a) Isosteric heats of  $\text{CO}_2$  adsorption on ZIF-8 and 2ZNC-organic compounds; (b) Isosteric heats of  $\text{CO}_2$  adsorption on 2ZNC-inorganic compounds.

**Table S1.** The CO<sub>2</sub> adsorption performance of 2ZNC-KHCO<sub>3</sub>-600 and similar materials reported in the literature.

Sample	Original material	CO <sub>2</sub> adsorption capacity at 1 bar (mmol/g)		Reference
		0 °C	25 °C	
2ZNC-KHCO <sub>3</sub> -600	ZIF-8	6.55	4.60	This work
ZIF-8/Pan	ZIF-8	/	4.20	[2]
20-ZCMC-800	ZIF-8	7.30	4.26	[3]
HNC-350-850	ZIF-8	6.21	3.56	[4]
2CN61-KCl-700	ZIF-61	6.19	3.91	[5]
mJUC160-900	JUC-160	5.50	3.50	[6]
5C-C <sub>6</sub> H <sub>14</sub> O <sub>6</sub> -900	MOF-5	5.18	3.32	[7]
CS3K0U800	Glucose	6.67	4.26	[8]
NSDCS2700	Glucose	5.60	3.40	[9]
MNC-0-800	Magnesium gluconate	6.60	4.22	[10]
CN6-750-KOH	Biomass	5.57	3.91	[11]
OPMK-900	Biomass	6.67	3.97	[12]
LC-C22	Biomass	4.89	4.23	[13]
HSM-550-2	Biomass	6.34	4.23	[14]

**Table S2.** The contents of C, N, O, Zn in all samples based on XPS characterizations.

Sample	C (wt%)	N (wt%)	O (wt%)	Zn (wt%)
ZIF-8	68.43	18.44	6.25	6.88
ZNC-600	68.82	20.36	9.75	1.07
2ZNC-C <sub>9</sub> H <sub>6</sub> O <sub>6</sub> -600	65.19	20.22	10.87	3.72
2ZNC-C <sub>3</sub> H <sub>2</sub> N <sub>2</sub> -600	67.81	20.46	9.50	2.23
2ZNC-C <sub>16</sub> H <sub>32</sub> O <sub>2</sub> -600	66.23	21.24	10.78	1.75
2ZNC-C <sub>12</sub> H <sub>22</sub> O <sub>11</sub> -600	71.27	17.33	9.99	1.41
2ZNC-C <sub>2</sub> H <sub>4</sub> N <sub>4</sub> -600	66.87	23.67	7.97	1.49
2ZNC-C <sub>3</sub> H <sub>6</sub> N <sub>6</sub> -600	68.89	23.03	6.74	1.34
2ZNC-Na <sub>3</sub> PO <sub>4</sub> -600	65.50	22.83	8.99	2.68
2ZNC-Na <sub>2</sub> SO <sub>4</sub> -600	64.76	22.70	11.29	1.25
2ZNC-CH <sub>3</sub> COONa-600	68.08	22.01	8.12	1.79
2ZNC-KOH-600	63.93	23.54	11.25	1.28
2ZNC-Na <sub>2</sub> CO <sub>3</sub> -600	66.71	21.74	10.36	1.19
2ZNC-KHCO <sub>3</sub> -600	63.27	23.35	12.15	1.23

**Table S3.** BET specific surface area ( $S_{BET}$ ), total pore volume ( $V_{total}$ ), Porosity, and cumulative pore volume in the range of 0–20 Å, 0–10 Å and 5–7 Å of all samples.

Sample	$S_{BET}$ (m <sup>2</sup> /g)	$V_{total}$ (cm <sup>3</sup> /g)	Porosity (%)	$V_{micro}$ (cm <sup>3</sup> /g)	Cumulative pore volume (cm <sup>3</sup> /g)		
					5–7(Å)	7–9(Å)	0–10(Å)
ZIF-8	1422.2111	0.582	36.79	0.471	0	0	0.291
ZNC-600	152.0762	0.230	18.70	0.042	0.018	0.011	0.031
2ZNC-C <sub>9</sub> H <sub>6</sub> O <sub>6</sub> -600	14.0545	0.010	0.99	0.004	0	0	0
2ZNC-C <sub>3</sub> H <sub>2</sub> N <sub>2</sub> -600	119.1156	0.121	10.79	0.032	0.013	0.010	0.023
2ZNC-C <sub>16</sub> H <sub>32</sub> O <sub>2</sub> -600	90.057	0.124	11.03	0.020	0	0.009	0.009
2ZNC-C <sub>12</sub> H <sub>22</sub> O <sub>11</sub> -600	213.34	0.108	9.75	0.060	0	0.048	0.048
2ZNC-C <sub>2</sub> H <sub>4</sub> N <sub>4</sub> -600	522.3894	0.653	39.50	0.135	0.062	0.053	0.116
2ZNC-C <sub>3</sub> H <sub>6</sub> N <sub>6</sub> -600	571.2232	0.476	32.25	0.149	0.078	0.042	0.120
2ZNC-Na <sub>3</sub> PO <sub>4</sub> -600	617.3971	0.482	32.52	0.174	0.025	0.137	0.162
2ZNC-Na <sub>2</sub> SO <sub>4</sub> -600	808.6519	0.376	27.33	0.257	0.041	0.161	0.202
2ZNC-CH <sub>3</sub> COONa-600	1052.075	0.393	28.21	0.341	0.045	0.258	0.302
2ZNC-KOH-600	1020.1166	0.367	26.85	0.353	0.177	0.111	0.301
2ZNC-Na <sub>2</sub> CO <sub>3</sub> -600	1095.0764	0.497	33.20	0.361	0.187	0.108	0.295
2ZNC-KHCO <sub>3</sub> -600	1179.73	0.466	31.79	0.388	0.025	0.294	0.320

**Table S4.** The carbon yields of ZNCs.

Sample	Carbon yield (wt%)
ZNC-600	34
2ZNC-C <sub>9</sub> H <sub>6</sub> O <sub>6</sub> -600	36
2ZNC-C <sub>3</sub> H <sub>2</sub> N <sub>2</sub> -600	50
2ZNC-C <sub>16</sub> H <sub>32</sub> O <sub>2</sub> -600	38
2ZNC-C <sub>12</sub> H <sub>22</sub> O <sub>11</sub> -600	42
2ZNC-C <sub>2</sub> H <sub>4</sub> N <sub>4</sub> -600	44
2ZNC-C <sub>3</sub> H <sub>6</sub> N <sub>6</sub> -600	45
2ZNC-Na <sub>3</sub> PO <sub>4</sub> -600	51
2ZNC-Na <sub>2</sub> SO <sub>4</sub> -600	43
2ZNC-CH <sub>3</sub> COONa-600	48
2ZNC-KOH-600	54
2ZNC-Na <sub>2</sub> CO <sub>3</sub> -600	46
2ZNC-KHCO <sub>3</sub> -600	57

**Table S5.** CO<sub>2</sub> adsorption capacity of samples at 25 °C and 0 °C (1 bar).

Sample	CO <sub>2</sub> adsorption capacity at 1 bar (mmol/g)	
	0 °C	25 °C
ZIF-8	1.69	0.43
ZNC-600	2.58	1.81
2ZNC-C <sub>9</sub> H <sub>6</sub> O <sub>6</sub> -600	1.83	1.40
2ZNC-C <sub>3</sub> H <sub>2</sub> N <sub>2</sub> -600	1.86	1.44
2ZNC-C <sub>16</sub> H <sub>32</sub> O <sub>2</sub> -600	2.05	1.55
2ZNC-C <sub>12</sub> H <sub>22</sub> O <sub>11</sub> -600	2.31	1.95
2ZNC-C <sub>2</sub> H <sub>4</sub> N <sub>4</sub> -600	3.54	2.51
2ZNC-C <sub>3</sub> H <sub>6</sub> N <sub>6</sub> -600	3.31	3.03
2ZNC-Na <sub>3</sub> PO <sub>4</sub> -600	4.04	3.09
2ZNC-Na <sub>2</sub> SO <sub>4</sub> -600	3.55	3.41
2ZNC-CH <sub>3</sub> COONa-600	5.51	4.07
2ZNC-KOH-600	5.37	4.41
2ZNC-Na <sub>2</sub> CO <sub>3</sub> -600	5.48	4.52
2ZNC-KHCO <sub>3</sub> -600	6.55	4.60

**Table S6.** The content of different chemical states of N element before and after CO<sub>2</sub> adsorption on 2ZNC-KHCO<sub>3</sub>-600.

2ZNC-KHCO <sub>3</sub> -600	Pyridine-N (wt%)	Pyrrole-N (wt%)	Graphitic-N (wt%)	Oxide-N (wt%)
after adsorption of CO <sub>2</sub>	6.48	6.66	7.24	2.07
before adsorption of CO <sub>2</sub>	6.95	6.35	7.77	2.28

**Table S7.** The content of different chemical states of O element before and after CO<sub>2</sub> adsorption on 2ZNC-KHCO<sub>3</sub>-600.

2ZNC-KHCO <sub>3</sub> -600	quinones (wt%)	COOH (wt%)	C=O (wt%)	C-O (wt%)	O-H (wt%)
after adsorption of CO <sub>2</sub>	3.07	4.06	1.87	0.95	1.60
before adsorption of CO <sub>2</sub>	3.06	4.12	2.29	1.06	1.62

**Table S8** The contents of N elements of different chemical states in ZNCs.

Sample	Pyridine-N (wt%)	Pyrrole-N (wt%)	Graphitic-N (wt%)	Oxide-N (wt%)
ZNC-600	6.12	5.23	7.48	1.53
2ZNC-C <sub>9</sub> H <sub>6</sub> O <sub>6</sub> -600	6.90	4.99	7.10	1.23
2ZNC-C <sub>3</sub> H <sub>2</sub> N <sub>2</sub> -600	8.22	4.97	5.91	1.36
2ZNC-C <sub>16</sub> H <sub>32</sub> O <sub>2</sub> -600	8.04	5.71	6.38	1.11
2ZNC-C <sub>12</sub> H <sub>22</sub> O <sub>11</sub> -600	6.18	4.48	5.86	0.81
2ZNC-C <sub>2</sub> H <sub>4</sub> N <sub>4</sub> -600	9.59	5.65	7.11	1.32
2ZNC-C <sub>3</sub> H <sub>6</sub> N <sub>6</sub> -600	8.82	5.76	6.78	1.67
2ZNC-Na <sub>3</sub> PO <sub>4</sub> -600	9.53	7.32	5.22	0.76
2ZNC-Na <sub>2</sub> SO <sub>4</sub> -600	7.62	5.69	7.95	1.44
2ZNC-CH <sub>3</sub> COONa-600	8.80	6.07	6.19	0.95
2ZNC-KOH-600	7.20	6.82	8.08	1.44
2ZNC-Na <sub>2</sub> CO <sub>3</sub> -600	6.96	6.73	7.21	0.84
2ZNC-KHCO <sub>3</sub> -600	6.95	6.35	7.77	2.28

**Table S9** Contents of O elements of different chemical states in ZNCs.

Sample	quinones (wt%)	COOH (wt%)	C=O (wt%)	C-O (wt%)	O-H (wt%)
ZNC-600	3.85	2.62	1.01	1.44	0.83
2ZNC-C <sub>9</sub> H <sub>6</sub> O <sub>6</sub> -600	4.49	2.97	1.93	0.75	0.73
2ZNC-C <sub>3</sub> H <sub>2</sub> N <sub>2</sub> -600	3.48	3.10	0.98	0.93	1.01
2ZNC-C <sub>16</sub> H <sub>32</sub> O <sub>2</sub> -600	4.80	2.22	1.49	1.20	1.07
2ZNC-C <sub>12</sub> H <sub>22</sub> O <sub>11</sub> -600	4.03	2.02	1.35	1.21	1.38
2ZNC-C <sub>2</sub> H <sub>4</sub> N <sub>4</sub> -600	2.15	1.51	1.36	2.02	0.93
2ZNC-C <sub>3</sub> H <sub>6</sub> N <sub>6</sub> -600	2.11	2.14	0.89	0.76	0.84
2ZNC-Na <sub>3</sub> PO <sub>4</sub> -600	3.71	2.07	0.86	0.96	1.39
2ZNC-Na <sub>2</sub> SO <sub>4</sub> -600	4.48	3.39	1.41	0.67	1.34
2ZNC-CH <sub>3</sub> COONa-600	2.77	3.20	1.07	0.59	0.49
2ZNC-KOH-600	2.70	3.89	1.45	1.00	2.24
2ZNC-Na <sub>2</sub> CO <sub>3</sub> -600	2.78	3.39	1.37	1.13	1.69
2ZNC-KHCO <sub>3</sub> -600	3.06	4.12	2.29	1.06	1.62

**Table S10.** Results of Lasso regression analysis.

	Non-standardized coefficient	standardized coefficient	P
constant	1.132	-	0.158
$V_{0-10(\text{\AA})}$	9.034	0.975	0.000
$V_{7-9(\text{\AA})}$	0.000	-0.041	1.000
Pyrrolic content	0.059	0.047	0.645
COOH content	0.000	-0.033	1.000
O-H content	0.076	0.050	0.691
$R^2$		0.980	

# References

- [1] M. Wang, Z. Xu, J. Fu, H. Du, S. Wang, Effect of chemical activators on polyphosphazene-based hierarchical porous carbons and their good CO<sub>2</sub> capture, *Diam. Relat. Mat.*, 125 (2022) 108966. 10.1016/j.diamond.2022.108966.
- [2] Y. Chiang, W. Chin, Preparation of Zeolitic Imidazolate Framework-8-Based Nanofiber Composites for Carbon Dioxide Adsorption, *Nanomaterials*, 12 (2022) 1492. 10.3390/nano12091492.
- [3] Y. Shu, L. Qiao, J. Geng, C. Li, B. Chen, Q. Wang, H. Uyama, Y. Shen, A novel ZIF-8@cellulose composite monolithic carbon via a facile template-free strategy for selective and efficient CO<sub>2</sub> adsorption, *Chem. Eng. J.*, 488 (2024) 151079. <https://doi.org/10.1016/j.cej.2024.151079>.
- [4] L. Qiao, Y. Shu, Y. Gao, H. Fan, J. Zhao, J. Zhang, H. Uyama, Y. Shen, Hierarchically N-doped porous carbon synthesized from 3D cellulose alcogel decorated by in-situ growth of ZIF-8 for high performance CO<sub>2</sub> capture, *Journal of Environmental Chemical Engineering*, 12 (2024) 114133. 10.1016/j.jece.2024.114133.
- [5] Y. Wang, Y. Suo, Y. Xu, Z. Zhang, Enhancing CO<sub>2</sub> adsorption performance of porous nitrogen-doped carbon materials derived from ZIFs: Insights into pore structure and surface chemistry, *Sep. Purif. Technol.*, 335 (2024) 126117. 10.1016/j.seppur.2023.126117.
- [6] Y. Pan, M. Xue, M. Chen, Q. Fang, L. Zhu, V. Valtchev, S. Qiu, ZIF-derived in situ nitrogen decorated porous carbons for CO<sub>2</sub> capture, *Inorg. Chem. Front.*, 3 (2016) 1112-1118. 10.1039/C6QI00158K.
- [7] Y. Wang, J. Xu, X. Lin, B. Wang, Z. Zhang, Y. Xu, Y. Suo, Facile synthesis of MOF-5-derived porous carbon with adjustable pore size for CO<sub>2</sub> capture, *J. Solid State Chem.*, 322 (2023) 123984. 10.1016/j.jssc.2023.123984.
- [8] J. Shi, H. Cui, J. Xu, N. Yan, Carbon spheres synthesized from KHCO<sub>3</sub> activation of glucose derived hydrochar with excellent CO<sub>2</sub> capture capabilities at both low and high pressures, *Sep. Purif. Technol.*, 294 (2022) 121193. 10.1016/j.seppur.2022.121193.
- [9] H. Cui, J. Xu, J. Shi, N. Yan, C. Zhang, S. You, N, S co-doped carbon spheres synthesized from glucose and thiourea as efficient CO<sub>2</sub> adsorbents, *J. Taiwan Inst. Chem. Eng.*, 138 (2022) 104441. 10.1016/j.jtice.2022.104441.
- [10] J. Shi, J. Xu, H. Cui, N. Yan, R. Yan, Y. Weng, NaCl template synthesis of N-doped porous carbon from magnesium gluconate for efficient CO<sub>2</sub> adsorption, *Sep. Purif. Technol.*, 355 (2025) 129756. 10.1016/j.seppur.2024.129756.
- [11] J. Li, A. Bao, J. Chen, Y. Bao, A green route to CO<sub>2</sub> adsorption on biomass chitosan derived nitrogen-doped micropore-dominated carbon nanosheets by different activators, *Journal of environmental chemical engineering*, 10 (2022) 107021. 10.1016/j.jece.2021.107021.
- [12] A. Rehman, G. Nazir, K.Y. Rhee, S. Park, Valorization of orange peel waste to tunable heteroatom-doped hydrochar-derived microporous carbons for selective CO<sub>2</sub> adsorption and separation, *Sci. Total Environ.*, 849 (2022) 157805. 10.1016/j.scitotenv.2022.157805.
- [13] L. Shao, H. Wan, L. Wang, J. Wang, Z. Liu, Z. Wu, P. Zhan, L. Zhang, X. Ma, J. Huang, N-doped highly microporous carbon derived from the self-assembled lignin/chitosan composites beads for selective CO<sub>2</sub> capture and efficient p-nitrophenol adsorption, *Sep. Purif. Technol.*, 313 (2023) 123440. 10.1016/j.seppur.2023.123440.
- [14] R. Pang, T. Lu, J. Shao, L. Wang, X. Wu, X. Qian, X. Hu, Highly Efficient Nitrogen-Doped Porous

Carbonaceous CO<sub>2</sub> Adsorbents Derived from Biomass, Energy Fuels, 35 (2021) 1620-1628.  
10.1021/acs.energyfuels.0c03832.